DINAME 2023 - Proceedings of the XIX International Symposium on Dynamic Problems of Mechanics,
A.S. De Paula, A.T. Fabro and M.R. Machado (Editors), ABCM.
Pirenópolis, Go, Brazil, February 26th to March 3rd, 2023

Design and experimental tests of a Superelastic Pitch Link with Shape Memory Alloy to vibration reduction in helicopters

[1]Andersson Guimarães Oliveira, andersson.oliveira@ceca.ufal.br, [2]Marcelo Cavalcanti Rodrigues, marcelo.labii@gmail.com, [3]Antonio Almeida Silva, antonio.almeida@ufcg.edu.br

[1]Federal University of Alagoas, Center of Engineer and Agricultural Sciences - BR104, Km85, Rio Largo - AL
[2]Federal University of Paraiba, Post Graduate Program in Mechanical Engineer - Cidade Universitaria - PB,
[3]Federal University of Campina Grande, Post Graduate Program in Mechanical Engineer - Av. Aprígio Veloso, 882 - Universitário, Campina Grande - PB

Abstract: Devices to control vibration in helicopters employs since passive to active strategies using common engineering materials, but might have improved by using of shape memory alloys as superelastic material. About helicopters, the vibration suppression is a goal pursued in all the projects, which represents a technological challenge, mainly when acting in rotating parts. One of requirements in this type of application is the developing of systems with low weight addition. Aligning the successfully applications in vibration suppression and the low weight, a superelastic material, Shape Memory Alloys (SMA) represents a properly candidate as a vibration absorber in rotating parts. The SMA take advantage from the superelastic behavior that dissipate energy due to a solid-state phase transformation. Thus, this paper presents a SMA device (Superelastic Pitch Link), developed and tested in bench to be designed as a mechanism towards vibration suppression in helicopter blades. The experimental results demonstrate, in comparative analysis, the hysteretic behavior of an 11g device and energy dissipation until $0.26MJ/m^3$.

Keywords: helicopter vibration supression, shape memory alloy, superelasticity, Superelastic pitch link

INTRODUCTION

One of the vibration sources in helicopters are placed in the main rotor. Due to the aerodynamic interactions in its blades, vibrations take place on the blades and are transmitted to the fuselage through the main shaft. The amount of strategies focused in the blades to vibrating control is named Individual Blade Control (IBC). The IBC is based on apply systems to vibrating reduction by devices incorporated in the rotating parts, above the swashplate, a component that represents the frontier between rotating and non-rotating parts in the aircraft, depicted in the illustration of Fig. 1. In this sense, the IBC control may be employed in solutions with material witch changes its shape and stiffness, as exemplified by Shape Memory Alloys (SMA): used in morphing blades design. In addition, it´s possible to take advantage of superelasticity properties, by its capacity to dissipate energy under mechanical strain, tapped to perform vibration absorbers. The SMA is employed in a variety of engineering applications, among these, vibrations control (Reis *et al.*, 2019). The solid-state phase transformation makes possible both the modal shapes changing (Shape Memory Effect) (SMA-ME), and energy dissipation as a damper thought stress (Superelastic Effect), indicated as (SMA-SE) (Lagoudas, 2008).

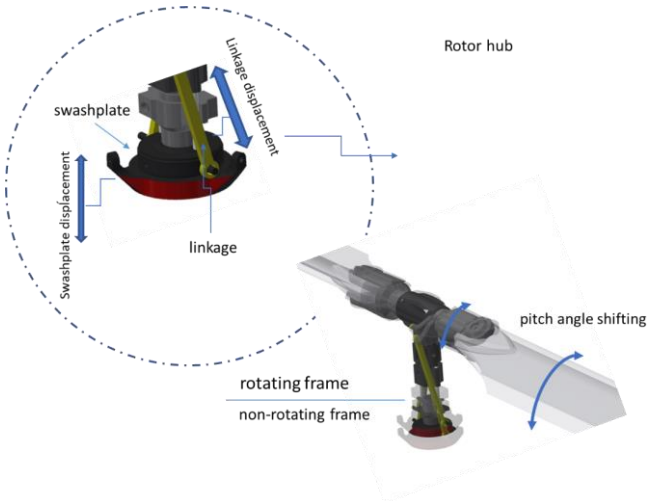

Figure 1 - Rotor rub basic mechanism. The author.

The current helicopter vibration control systems employs base isolators, hydraulic actuators, and tuned mass dampers (TMD), among other technics (Welsh, 2018). Concerning superelastic materials to helicopters vibration, in general, literature reports piezoelectricity solution and SMA-ME in morphing systems (Prahlad and Chopra, 2001; Madsen, Clingman and Bushnell, 2013; Lynch *et al.*, 2016). Based on vibration control with SMA-ME, vibration control technics employ active systems to induce phase transformation, in most the examples by joule effect. Regarding SMA-SE, is necessary enough stress to induce phase transformation and blend the proper geometry with the displacement to reach efficient energy dissipation.

Thus, in this paper, it´s possible to match the SMA properties with helicopter problems, towards reducing vibrations and its undesirable effects in order to propose a geometry of superelastic pitch link that may be tested using SMA springs. In this sense, the objective is design a device to vibration control in helicopters blades by stiff pitch link replacement. In other words, the device named superelastic pitch link can replace the stiff pitch link. Yet, before the installation of a device in a real helicopter rotor, it´s necessary perform bench tests to ensure the energy dissipation and carry out geometry improvements.

The component pitch link

The maneuvers of a helicopter depend on cyclic or collective variations in the pitch angle of its blades. The commands to promote theses pitch angle shifting are originated from the pilot, transmitted by mechanisms from non-rotating frame to the rotate frame (rotor). Pitch link are stiff rods which transmits the commands to pitch angle shifting of the blades. The vibrations originated on the blades are transmitted to the aircraft through the main shaft (for main rotor) and pitch links (Bramwell, Done and Balmford, 2001). Due to the neglected damping capacity of stiff pitch links, no energy dissipation carries out in the system.

The illustration of Fig. 2 shows one example of pitch link positioning: one pitch link of a helimodel T-Rex 500, that although belongs to a helimodel for hobby, employs the same mechanism of a real aircraft and motivates its use for bench tests. Pitch links are fabricated with stiff rods, so that, in this research, conventional pitch links are named stiff pitch links in order to compare with superelastic pitch link designed.

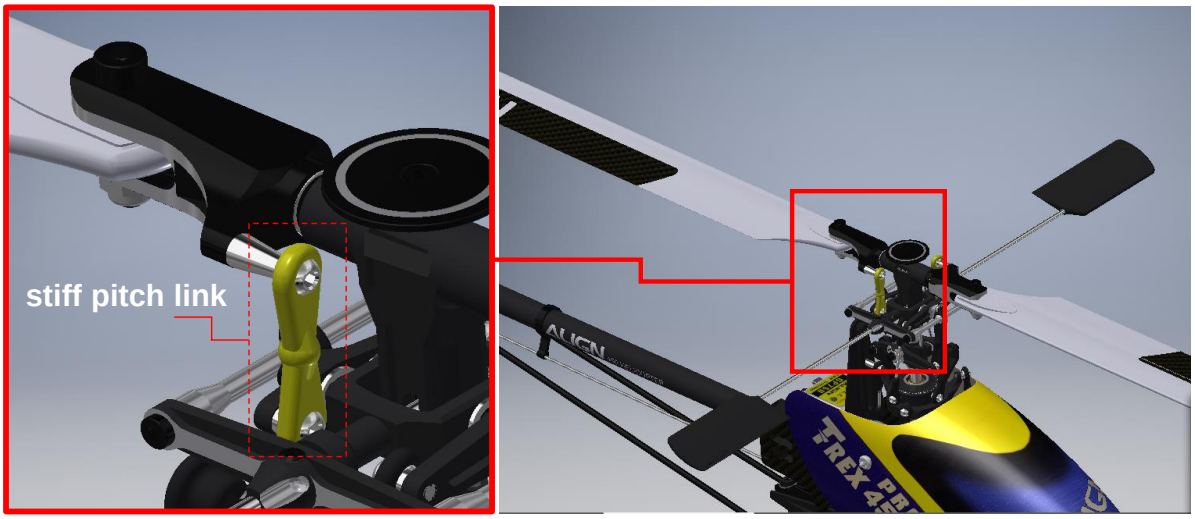

Figure 2 – Example of Stiff pitch link positioning employed in a helimodel T-Rex 500.

Rotor hub characterization

The rotor hub prototype, from commercial helimodel T-Rex 500, was characterized and detailed in Rosata(2015), which kinematic analysis grounded the scheme of the prototype depicted in Fig.3b.

Considering no geometry modifications in the original rotor hub, it's important to follow the original dimensions of the prototype and evaluate the available space to perform the pinch link replacement. The dimensions and positions of elements depicted in Fig. 3 are listed in the Table 1. The rod l_2 corresponds to the stiff pitch link length that should be followed to evaluate the available space to design the superelastic pitch link. Thus, the distance between eyelets that link the blades and the bar of segment $\overline{AB}$ (Fig.3b) has to be preserved and the superelastic pitch link.

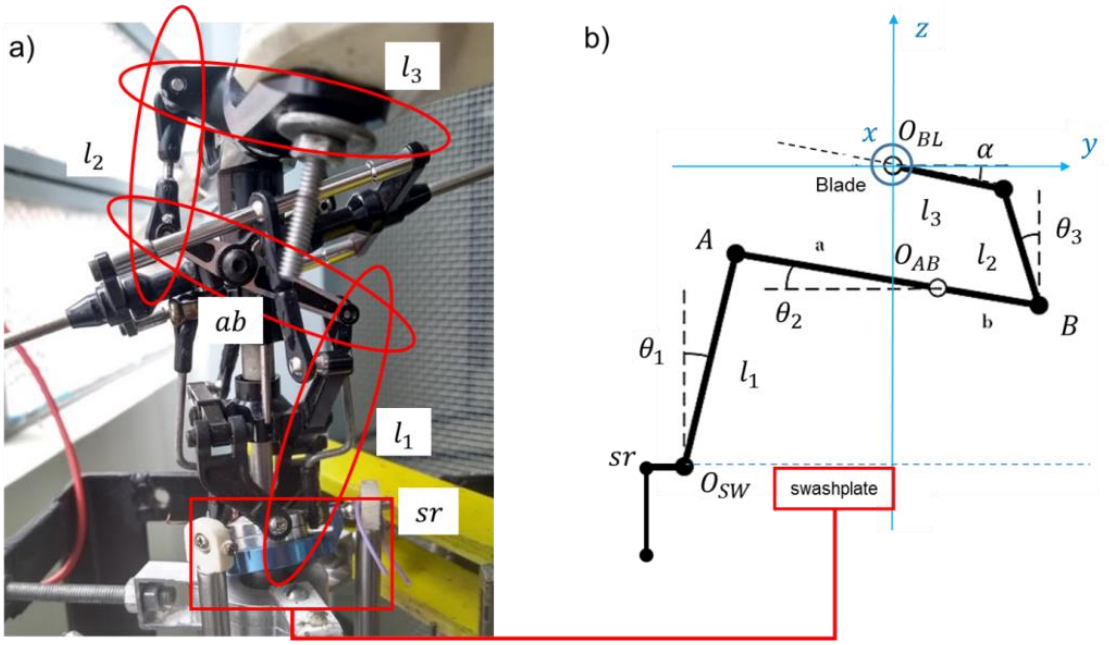

Figure 3 – Blade mechanism detail and cinematic diagram: a) mechanism links tags of prototype b) kinematic diagram, adapted from *Rosata (2015)*.

Table 1 – List of parameters of blade mechanism according to the tag in Figure 3

Parameter	Value	Description
l_1	49.50mm	Length of rod l_1
l_2	**25.30mm**	**Length of rod l_2 (stiff pitch link length)**
l_3	17.00mm	Length of rod l_3
a	25.20mm	Length of arm a
b	13.80mm	Length of arm b
O_{sw}	-	Position of swashplate linkage ball
α	$0-12^0$	Blade angle of attack
θ_1	-	Angle of rod l_1
θ_2	-	Angle of segment AB
θ_3	-	Angle of rod l_2
O_{BL}	0	Position of O_{BL} in x, y, z

Superelastic pitch link Design

Taking into account the geometric requirements of space and clearance available of the stiff pitch link rod, the proposed device preserves the stiff pitch link length and original attachment with eye bolt. Based on successful researches of Anusonti-Inthra(2000), Nitzsche(2015) and (Reis, 2018), was design a concept of device, which may replace the stiff pitch link in order to reduce vibration due to transmissibility from blade root to swash plate mechanism employing superelelastic SMA springs. The original concept of superelastic pitch link is depicted in Fig.4.

The model depicted in Fig.4 is evaluated before fabrication, so that the physical prototype presents few modifications when compared with the 3D mode, basically in springs attachment and the rocker arm attachment on the eyelet.

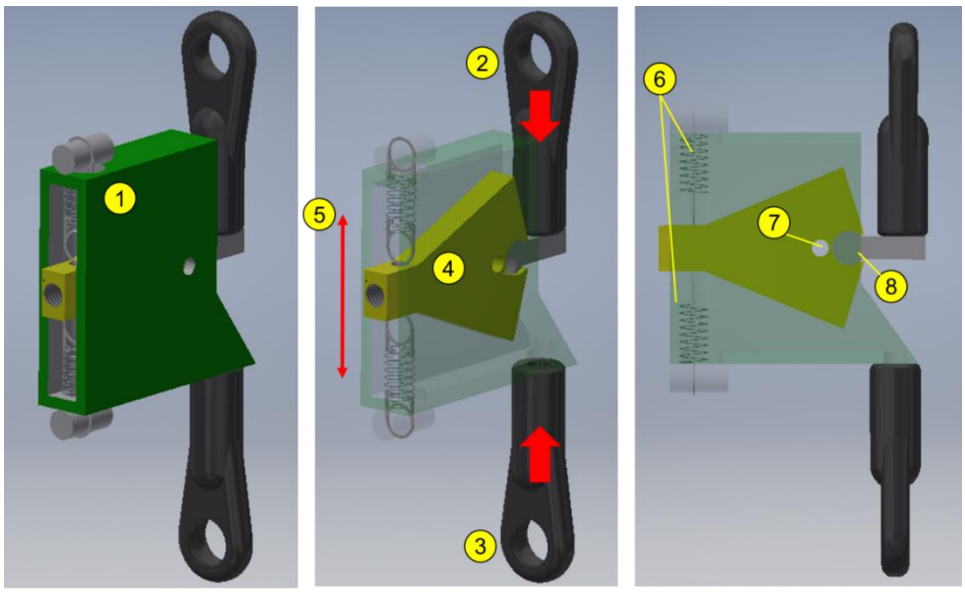

1 spring support
2 eyelet blade attachment
3 eyelet swashplate command attachment
4 rocker arm
5 elongation direction
6 SMA springs
7 rocker arm pin
8 eyelet base attachment

Figure 4 - SMA-SE device concept and the main parts of the mechanism

The SMA device works as a “SMA pitch link” employing two SMA-SE orthodontic springs (NiTi spring, model M9), installed in opposition, pulling a rocker arm. The longitudinal and relative displacement between the root blade attachment and the swashplate command is transmitted to the rocker arm, which converts this movement in elongation of the SMA-SE springs. The elongation of springs induces the phase transformation of SMA-SE, so that couple damping in the system. The SMA springs are commercial without any thermal treatment before installation. The demonstration of replacement from the stiff to SMA-SE pitch link, using a 3D model of T-Rex 500 hub head, is illustrated in Fig.5.

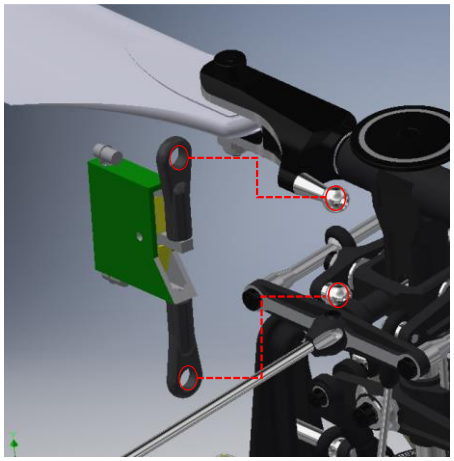

Figure 5 – Simulation of definitive positioning of SMA-SE pitch link

The SMA pitch link proposal has to mix two important and opposite requirements: ensure phase transformation of the material, by stress, and avoid large relative displacements between eyelets (points 2 and 3 in Fig.4). The strategy adopts geometry with asymmetry in the rocker arm pin position, so that amplify the small displacements of point 8 Fig.4). The geometry amplifies the input displacement in 3.37 times (calculated by the kinematic diagram of Fig.6), named as boost factor. When in equilibrium, the springs are assembled with deformation offset (pre-stroke) in 300%, setting the material in approximately the middle of the phase transformation region, even before dynamic operation, according to the strategies adopted by (Huang et al., 2014; Moraes et al., 2018; Reis, 2018).

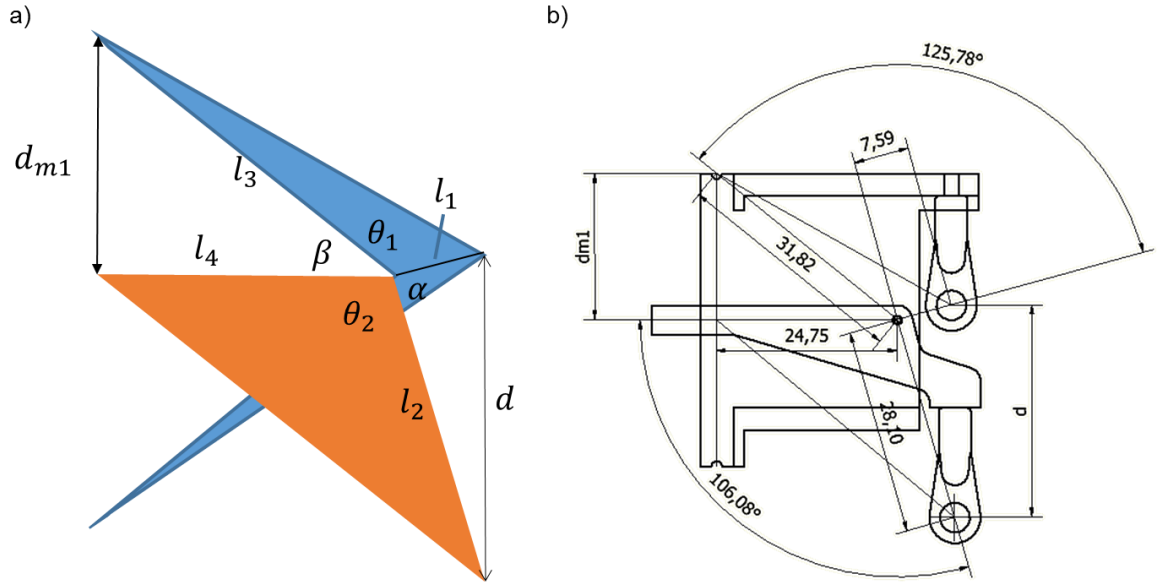

Figure 6 – SMA pitch link concept: a) cinematic kinematic diagram; b) dimensioning of prototype necessary to replace with original stiff pitch link.

To avoid interference in the synchronism of the blade mechanism, the SMA pitch link should not perform great lengths of shifting. Thus, the maximum displacement of SMA pitch link should be limited. On the other hand, the device amplifies the input displacement by a factor of 3.37, so that follows both criteria of low input displacement and spring large output deformation. The distance "d" not exceed the length of rod l_2 (Fig.3b)

The commercial orthodontic SMA springs were thermomechanical characterized, aiming the temperature phase transformation in order to verify the superelastic behavior under environmental temperature. Sample SMA Spring was analyzed by Differential Scanning Calorimeter (DSC) witch thermogram is depicted in Fig.7.

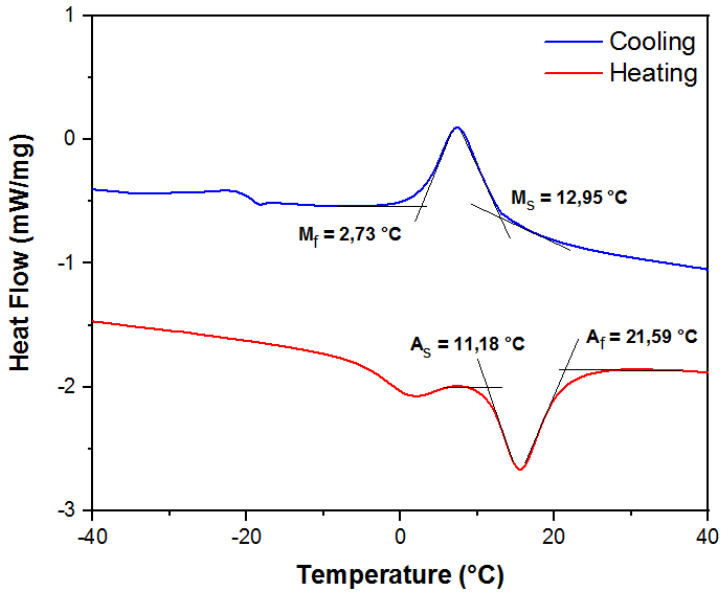

Figure 7 – Micro coil SMA spring thermogram from DSC testing.

During cooling, the material exhibit phase transformation from martensite to austenite ($M_s \rightarrow M_f$). In environmental temperature (21ºC) the material is completely austenitic ($A_s \rightarrow A_f$), which allows superelastic behavior. In laboratory is feasible to ensure temperatures above A_s, and superelestatic response. Yet, in real external application, the minimum distance between the environmental temperature and A_f has to pain attention. The DSC results indicates no additional thermal treatment needed before the prototype installation. Isothermal conditions are assumed once considering the superelastic effect.

EXPERIMENTAL RESULTS

The support of mechanism (Fig.8) is fabricated by additive manufacturing in PLA (Polylactic Acid). Using this SMA pitch link was performed experiments in order to analyze the coil spring assembling, carries out dynamic tests using modal shaker (forced vibration) to observes the hysteretic behavior of device.

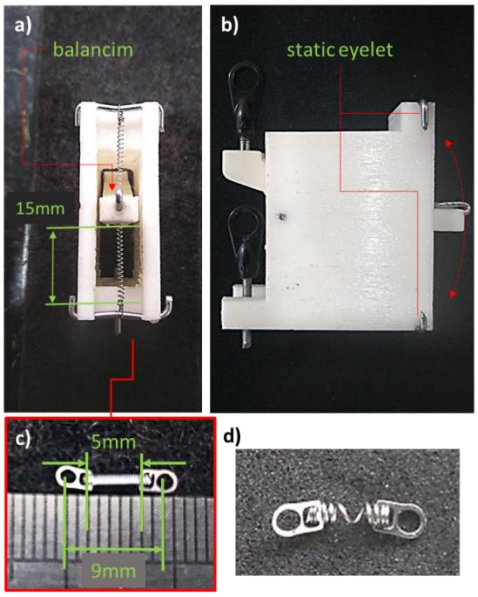

Figure 8 – SMA pitch link: a) PLA prototype (front view); b) PLA prototype (side view); c) dimensions of closed coil spring before assembly; c) distalizing spring (detail of one opened coil)

The position of the static eyelet determines de offset of the springs. In Fig.8c a detail of closed coil spring before offset demonstrates the initial length of each element. To obtain the length of 5mm the original M9 closed spring (Fig.8d) was sectioned so that employing 6 coils, as depicted. The bench tests performed with SMA pitch link employing the closed springs (Fig.8c) and was repeated with distalizing springs (Fig.8d).

The offset 15mm (Fig.8a) is adopted, both to closed spring and to distalizing spring (Fig.8d). The image of device ready to installing is exhibited in the Fig.9. The total mass consider the closed coil spring. The mass difference with when uses distalizing spring is about 7mg for each element.

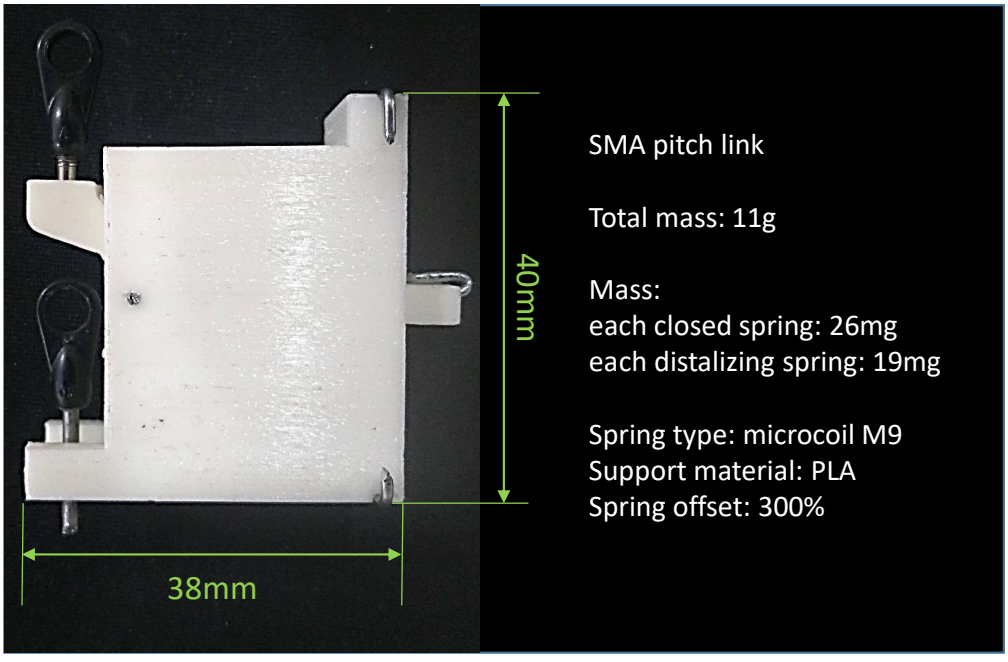

Figure 9 – SMA pitch link: general characteristics

The experimental data with SMA prototype, reported in literature, demonstrates maximum Superelastic deformation about 500% (Grassi *et al.*, 2015; Moraes *et al.*, 2018). In this particular application the maximum length of 25mm

(500%) may induce plastic deformation, an undesirable condition considering the geometric limitations. For safety, the available length of 15mm (offset in 300%) in the rocker arm its far from the plastic deformation and avoid permanent damages in the springs. Yet, the minimum input forces under device ensures hysteretic behavior of the SMA.

Dynamic tests with SMA pitch link

Before any forwarding test in a rotor hub prototype, a bench test performs input force and measure displacement to simulate the real operation. The kit employed (modal shaker, load cell and LVDT) is depicted in Fig.10.

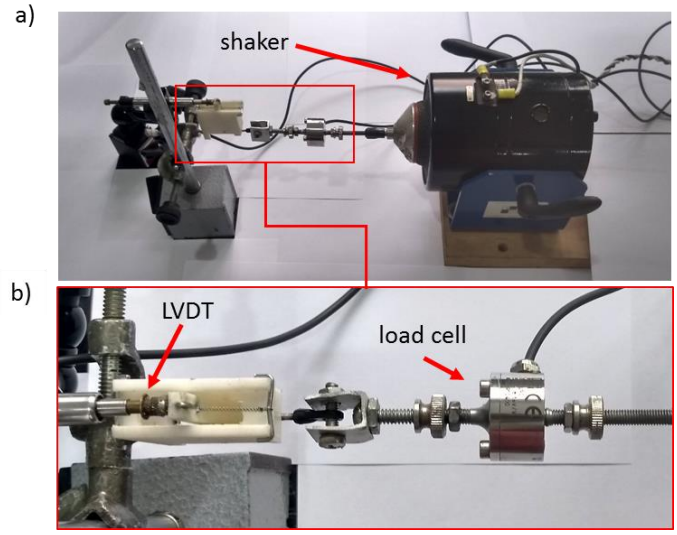

Figure 10 – Scheme for receptance measurements with SMA pitch link: a) assembly with modal shaker kit connected to device; b) detail indicating load cell and LVDT positioning.

The experiment generates the curve depicted in Fig.11 when the pitch link employs closed micro coil spring and in Fig.12 when the device employs distalizing micro coil spring. Both under a sinusoidal input signal, generating maximum peak force in approximately 2,5N. The graph exhibits the variation of distance between pitch link eyelets (distance *d*, depicted in Fig.6) for the correspondent input force. Because of LVDT positioning, in the opposed tip of balacim, a correction of the LVTD measurements, based on the boost factor calculates the effective displacement in *d*. Thus, the distance *d* and force F (load cell) generates the force/displacement curves.

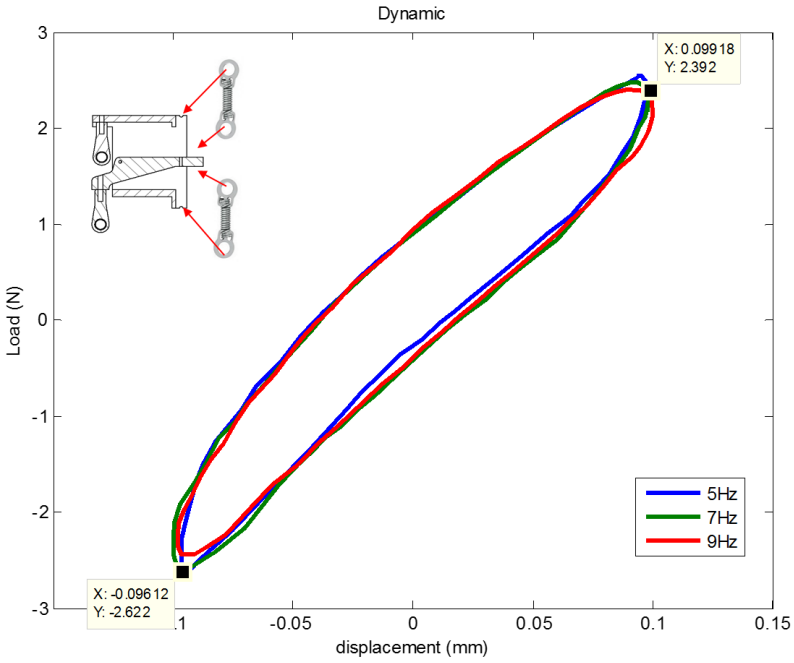

Figure 11 – Force/displacement curve of SMA pitch link employing closed coil spring with 300% offset.

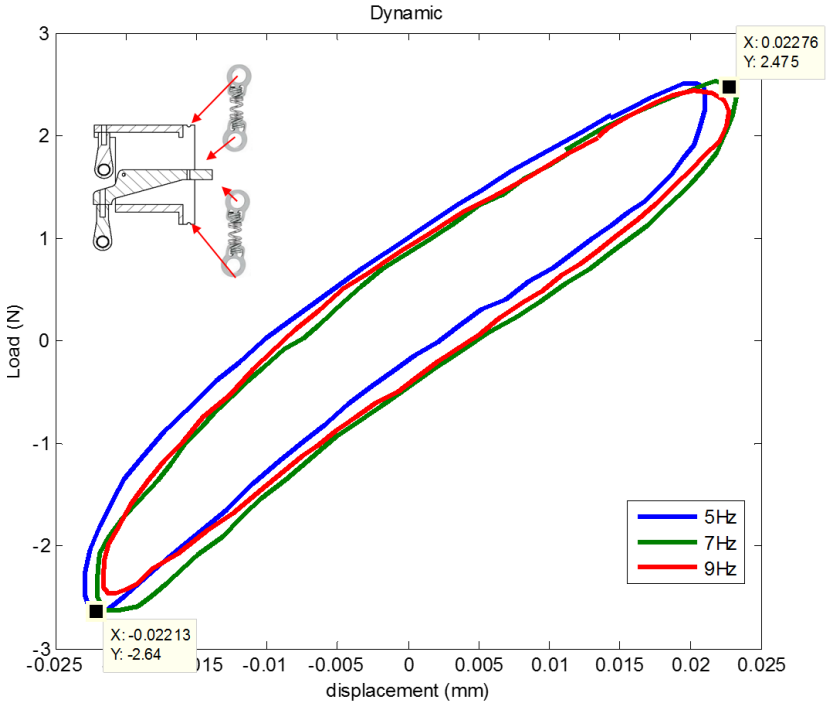

Figure 12 - Force/displacement curve of SMA pitch link employing distalizing coil spring with 300% offset.

The input frequencies in 5, 7, and 9Hz (interesting frequency span) were tested to verify the presence of hysteretic behavior. For all of these frequencies, the experiment indicates hysteresis, although the maximum device displacement, and consequently the springs, exceed about 10% of the offset (peak-to-peak). This result demonstrates the capacity of material's hysteretic behavior, even in lower displacement when adopted the strategy of pre-stroke due to the offset. The distance between eyelets did not exceed 0.20mm (peak-to-peak) for closed springs and did not exceed 0.05mm (peak-to-peak) for distalizing springs. Table 2 exhibits the dissipated energy and secant stiffness of each pitch link: employing closed and distalizing SMA springs. The dissipated energy represents an increase of about 2.33% with distalizing assembly compared with closed SMA springs. On the other hand, the stiffness rises 344% with distalizing SMA springs.

Table 2 – Dissipated energy and secant stiffness for each type of coil spring adopted in the SMA pitch link

	Spring type	Pitch link active coil spring volume (m^3)	Dissipated energy (MJ/m^3)	Pitch link stiffness (KN/m)
	Closed	$2.726 \cdot 10^{-9}$	0.257	25.67
	Distalizing	$0.964 \cdot 10^{-9}$	0.263	113.94

Fatigue tests with SMA coil springs

Taking into account that the main component of the SMA superelastic pitch link is the spring, closed and distalizing springs were tested in fatigue. The test was performed with each spring, without pitch link mechanism, to avoid influence of other movable parts. Each spring was subjected to amplitude of 1mm (peak-to-peak) under pre-strain in 300%, similar to when assembled in the pitch mechanism. To perform the fatigue tests with one constant frequency, was adopted 7Hz, according to the load tests of Fig.11 and Fig.12.

The functional fatigue was performed with an electrical mechanic shake table, model Shake Table II of manufacture Quanser. The experiment is depicted in Figure 13. In the experiment, the shake table performs the horizontal displacement, while one side of the support was attached on the table base and the other support end displaces under table movement according to a synodal signal in 1mm peak-to-peak amplitude, according to the expected operational conditions of SMA device. The displacement was measured with a displacement sensor LVDT. At the same time, a load cell registers the input force. The experiment was uninterrupted and performed under temperature of 21°C. The test took place with three units of each spring type.

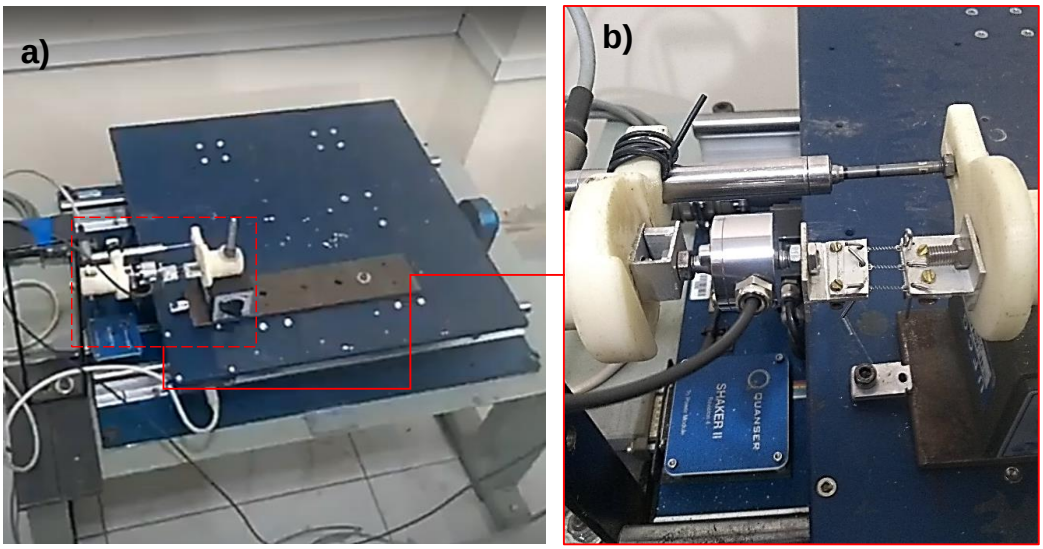

Figure 13 – Fatigue experiment in SMA springs: a) general view of shake table and supports assembly; b) assembly detail

The system HBM MX840A was employed as platform to record the sensors signal under a sample rate of 100Hz, so that the number of cycles was counted at the final test based on the test spent time.

The results are presented from Fig.14 to Fig.17. In both experiments, the springs were subjected to the same experimental parameters, differing only on spring type: closed and distalizing coil spring. For closed springs, the result of Fig.14 indicates the stabilized behavior from $2 \cdot 10^5$ cycles to $6 \cdot 10^5$cycles considering a stable maximum force for infinite cycles. The test was interrupted without structural failure in any specimen tested.

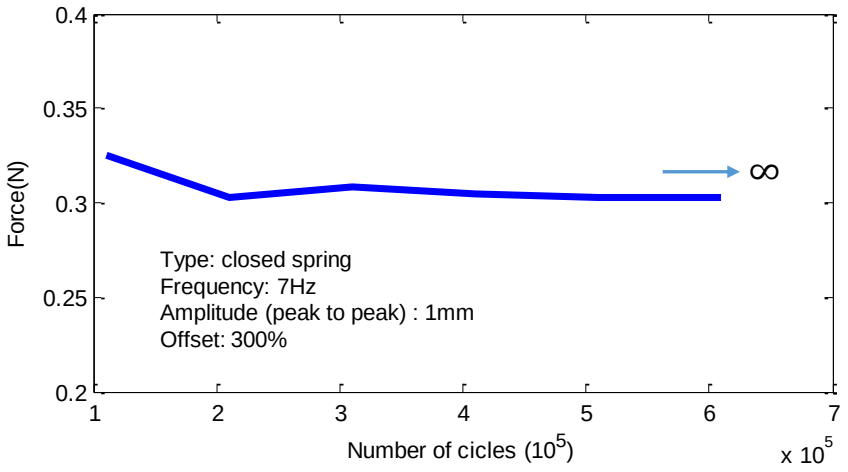

Figure 14 – Maximum peak force of closed coil spring under fatigue test stopped in $6 \cdot 10^5$ cycles, without structural failure

The force measured depends on the maximum elongation applied. This force tends to fall after the initial cycles and stabilizes until the end of the experiment. In Fig.15 is depicted the evolution of superelastic behavior of closed coil spring demonstrating the hysteretic behavior until the end of the test. Taking into account that the load cell operates under tension during all test long, the force was registered in negative values.

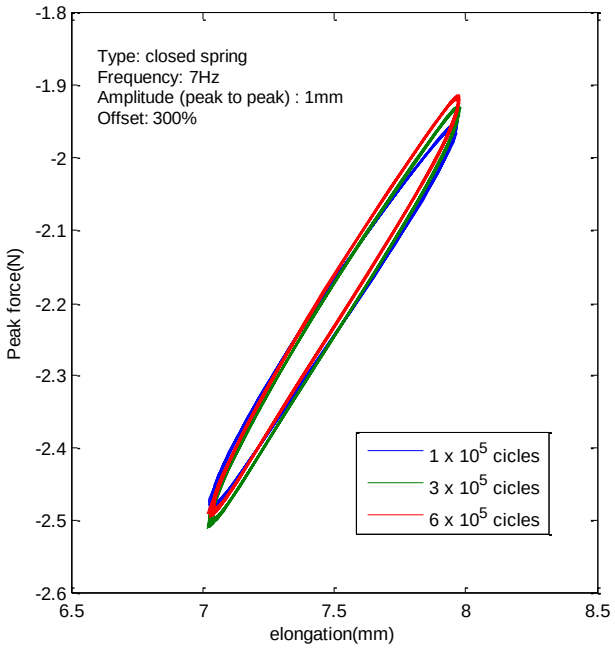

Figure 15 – Evolution of superelastic behavior of closed coil SMA spring with measurements stopped in $6 \cdot 10^5$ cycles without structural failure.

In Fig.16 is depicted the maximum peak force of fatigue test with distalizing springs. The test was interrupted due to structural failure that take place in about $0.6 \cdot 10^5$ cycles for wall the three specimens tested, exactly 10 times the less the closed springs. Similar to the Fig.15, the hysteretic behavior of the distalizing spring is depicted in Fig.17.

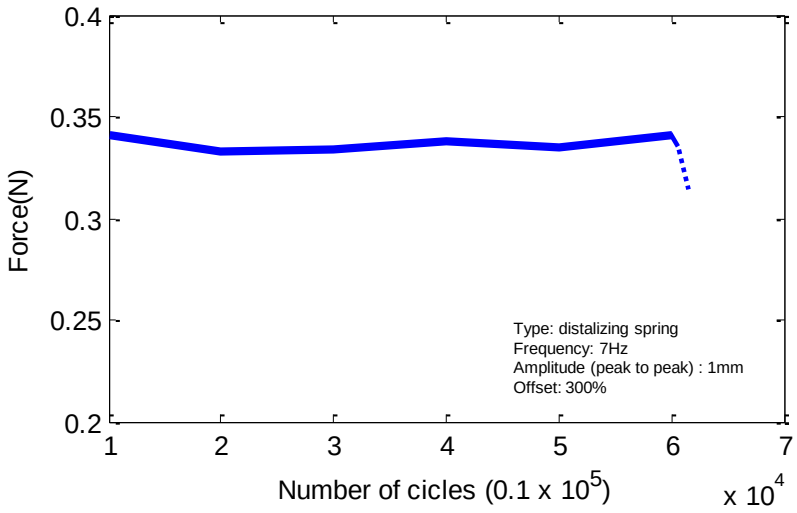

Figure 16 - Maximum peak force of distalizing SMA coil spring under fatigue test stopped in $6 \cdot 10^4$ cycles, after structural failure

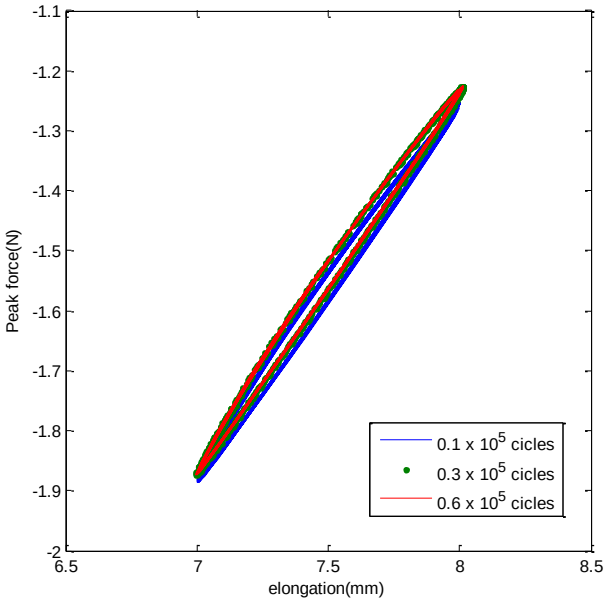

Figure 17 - Evolution of superelastic behavior of distalizing SMA coil spring with measurements stopped in $0.6 \cdot 10^5$ **cycles after structural failure.**

CONCLUSIONS

In energy dissipation wise, both superelastic pitch link version (with closed and distalizing springs) demonstrates few differences of 2.33%. Still, considering the requirement of low deformation using superelastic pitch link do make proximity of the stiff pitch link behavior, the rising stiffness of distalizing springs (344%) version suggests that this type of spring is, in time, the best choice for this pitch link geometry and proper to run forwarding tests in a helicopter prototype. Thus, the optimized version of superelastic pitch link may employ distalizing springs to ensure the highest stiffness combined with the proper energy dissipation. In terms of distalizing spring, is demanded less strain to induce phase transformation when compared with the closed spring for the same conditions. Otherwise, the fatigue life of superelastic pitch link with distalizing springs is reduced when compared with the superelastic pitch link employing the closed springs, as demonstrated by the results of Fig. and Fig.17.

The best results with the superelastic pitch link, under the configuration presented in the experimental tests, reach the maximum energy dissipation of $0.263 MJ/m^3$. Comparing these results with dissipated energy in preview researches, mainly those which uses micro coils SMA springs, as exhibited in Moraes (2017), was observed a maximum of $0.350 MJ/m^3$ in dissipated energy, considering dynamic loading under low frequency (about 3.25Hz). In the same field, (Reis *et al.*, 2019) obtains, results close to $1 MJ/m^3$, in dynamic loading (about 15Hz). Both results (greater than the obtained in the current research) subjects the microcoil springs to large deformations, what explain these energy dissipation values. Considering the dissipated energy, these results encourage the forward testing with this device installed in a whirl tower, in rotation, after superelastic pitch link geometry improvements, in order to observe the dynamic behavior simulating hover flight or forwarding flight, for example. At the same time, the concept of this research, considering the successful in bench results suggest the expansion of supereslatic pitch link employment in other mechanisms that uses pitch angle shifting, like helix propellers and areogenerators. Because of this, the superelastic pitch link concept was registered in the National Institute of Industrial Property (process number BR 10 2022 017269 2).

ACKNOWLEDGMENTS

The authors thank to the Integrity and Inspection Research Group (GPII), the Post Graduate Program of the Federal University of Paraiba (PPGEM/UFPB) and the Vibration and Instrumentation Laboratory of UFCG (LVI/UFCG). The authors gratefully acknowledge the financial support of Federal University of Paraiba and the National Council for Scientific and Technological Development (CNPQ), project number 408131/2018-7.

REFERENCES

Anusonti-Inthra, P. and Gandhi, F. (2000) ‘Helicopter vibration reduction through cyclic variations in rotor blade root stiffness’, *Journal of Intelligent Material Systems and Structures*, 11(2), pp. 153–166. doi: 10.1106/B8NQ-4LNN-MPPL-AFHV.

Bramwell, A. R. S., Done, G. and Balmford, D. (2001) *Bramwell's helicopter dynamics*. Second. Edited by Butterworth-Heinemann. Oxford: Butterworth-Heinemann.

Grassi, E. N. D. *et al.* (2015) 'Effect of heat treatments on the thermomechanical behaviour of Ni-Ti superelastic mini coil springs', *MATEC Web of Conferences*, 33. doi: 10.1051/matecconf/20153303004.

Lagoudas, D. C. (2008) *Shape Memory Alloys*. Dimitris C. Edited by L. Springer Science+Business Media. Boston, MA: Springer US. doi: 10.1007/978-0-387-47685-8.

Lynch, B. *et al.* (2016) 'Characterization, modeling, and control of Ni-Ti shape memory alloy based on electrical resistance feedback', *Journal of Intelligent Material Systems and Structures*, 27(18), pp. 2489–2507. doi: 10.1177/1045389X16633764.

Madsen, C. L., Clingman, D. J. and Bushnell, G. S. (2013) 'Shape Memory Alloy Active Spars for blade twist'. United States.

Moraes, Y. J. O. (2017) *Dynamical Analysis Applied to Control Passive of Vibrations in an Structural Device Incorporating Superelastic NiTi Mini Coil Springs*. Federal University of Campina Grande.

Moraes, Y. J. O. *et al.* (2018) 'Dynamical analysis applied to passive control of vibrations in a structural model incorporating SMA-SE coil springs', *Advances in Materials Science and Engineering*, 2018. doi: 10.1155/2018/2025839.

Nitzsche, F., D'Assunção, D. and De Marqui Junior, C. (2015) 'Aeroelastic control of non-rotating and rotating wings using the dynamic stiffness modulation principle via piezoelectric actuators', *Journal of Intelligent Material Systems and Structures*, 26(13), pp. 1656–1668. doi: 10.1177/1045389X15572011.

Prahlad, H. and Chopra, I. (2001) 'Design of a variable twist tilt-rotor blade using shape memory alloy (SMA) actuators', in Davis, L. P. (ed.) *SPIE's 8th Annual Conference Smart Structures and Materials*, pp. 46–59. doi: 10.1117/12.436559.

Reis, R. (2018) *Efeito da incorporação de minimolas NiTi superelásticas no amortecimento estrutural: aplicações em atenuação passiva de pás de aero gerador*. Universidade Federal de Campina Grande.

Reis, R. P. B. dos *et al.* (2019) 'Methodology for the estimation of material damping as applied to superelastic shape memory alloy mini-springs', *Materials and Design*, 161, pp. 124–135. doi: 10.1016/j.matdes.2018.11.012.

Rosata, P. (2015) *Identification of a small-scale helicopter dynamic model*. Università di Pisa.

Welsh, W. A. (2018) 'Helicopter Vibration Reduction', in *Morphing Wing Technologies*. Elsevier, pp. 865–892. doi: 10.1016/B978-0-08-100964-2.00027-7.

RESPONSIBILITY NOTICE

The author(s) is (are) the only responsible for the printed material included in this paper.